

Chemical Issues Addressing the Construction of the Distal Ni[Cysteine-Glycine-Cysteine]²⁻ Site of Acetyl CoA Synthase: Why Not Copper?

Kayla N. Green,[†] Scott M. Brothers,[†] Boram Lee,[‡] Marcetta Y. Darensbourg,[†] and David A. Rockcliffe^{*,‡}

Department of Chemistry, Texas A&M University, College Station, Texas 77845, and Division of Mathematics and Sciences, Kentucky State University, Frankfort, Kentucky 40601

Received August 27, 2008

The discovery of the metallopeptide Ni(Cysteine-Glycine-Cysteine)²⁻, Ni(CGC)²⁻, in the A-cluster active site of Acetyl CoA Synthase has prompted the synthesis of many small molecule models which employ M(N₂S₂) complexes as metalloligands. In vitro studies have shown that nickel incorporates into the N₂S₂ binding pocket even when copper is in the enzyme growth medium, while copper is preferentially taken up in the proximal site, displacing the catalytically active nickel. (Darnault, C.; Volbeda, A.; Kim, E.J.; Legrand, P.; Vernede, X.; Lindahl, P.A.; Fontecilla-Camps, J.C. *Nat. Struct. Biol.* **2003**, *10*, 271–279.) The work herein has been designed to address the chemical viability of copper(II) within the tripeptide N₂S₂ ligand set. To this end, a series of CuN₂S₂²⁻ complexes, the resin-bound, O-Cu(CGC)²⁻ (**A**) and free Cu(CGC)²⁻ (**B**) complexes, as well as Cu(ema)²⁻ (**C**) and Cu(emi)²⁻ (**D**) dianions, have been characterized by UV–vis, electron paramagnetic resonance (EPR), and electrospray ionization mass spectrometry (ESI-MS) spectroscopies, cyclic voltammetry (CV), and, where appropriate, X-ray diffraction studies, and compared to the Ni^{II} congeners. EPR spectroscopic results have indicated that, in frozen *N,N*-dimethylformamide (DMF) solution, the copper complexes are distorted square planar structures with nitrogen and sulfur donors. This is consistent with X-ray diffraction measurements which also show copper(II) in a distorted square planar environment that is bereft of CuN₂S₂²⁻ intermolecular interactions. Density-functional theory (DFT) calculations resulted in optimized structures that are consistent with crystallographic data and indicated highest occupied molecular orbital (HOMO)-singly occupied molecular orbital (SOMO) gaps of 5.01 and 4.68 eV for **C** and **D**, respectively. Optimized structures of Ni(ema)²⁻ and Ni(emi)²⁻ share the same basic characteristics as the copper(II) congeners. Electrochemical characterization of **C** and **D** resulted in a reversible Cu^{III/II} couple at –1.20 V and –1.40 V, respectively. Reactivity studies with Rh(CO)₂⁺ show similar donor capabilities for complexes **A–D**. Analysis of **A** shows that transmetalation does not occur. From competitive metal uptake studies on immobilized tripeptide it is concluded that the N₂S₂⁴⁻ ligating unit has a slight preference for Cu²⁺ over Ni²⁺ and that the biosynthetic pathway responsible for constructing the distal site of ACS must be selective for nickel insertion or copper exclusion, or both.

Introduction

The A-cluster active site of the bimetallic Ni enzyme, Acetyl CoA Synthase (ACS), shown in Figure 1, utilizes the metallopeptide Ni(Cysteine-Glycine-Cysteine)²⁻, Ni(CGC)²⁻, as a metallodithiolate ligand to the catalytically active metal center, denoted as M_p (p = proximal, with respect to the

4Fe4S cluster, refer to Figure 1), which, in the case of M_p = Ni, performs the organometallic chemistry required to assemble acetyl coenzyme A.^{1,2} Salient findings are that (a) the presence of nickel in both sites is required for catalytic activity; (b) Ni^{II} at the proximal position may be selectively removed and reconstituted or replaced by other metals,

* To whom correspondence should be addressed. E-mail: david.rockcliffe@kysu.edu.

[†] Texas A&M University.

[‡] Kentucky State University.

(1) Darnault, C.; Volbeda, A.; Kim, E. J.; Legrand, P.; Vernede, X.; Lindahl, P. A.; Fontecilla-Camps, J. C. *Nat. Struct. Biol.* **2003**, *10*, 271–279.

(2) Dokov, I. T.; Iverson, T. M.; Seravalli, J.; Ragsdale, S. W.; Drennan, C. L. *Science* **2002**, *298*, 567–572.

retaining Ni in the distal site; and (c) the enzyme was inactive when Cu^I or Cu^{II} was added to the nickel-depleted enzyme (It has been reasonably assumed that the removable or labile nickel is Ni_p, with no evidence of depletion at Ni_d).³ In addition, Zn^{II} substitution at the Ni_p position resulted in no catalytic activity.^{1,2} From these studies it was concluded that the active form of the ACS A-cluster contains a labile nickel center, Ni_p, that is replaceable by other metals.³ Nevertheless, nickel was purported to be the distal site metal in all reported structures even when copper or zinc was present in the growth media. Thus, a preference for nickel at this site is indicated.^{3,4}

Other metals (Co^{II} and Fe^{II}) have been found in a strikingly similar N₂S₂ Cys-Ser-Cys motif of Nitrile Hydratase, suggesting that the biological N₂S₂ ligation site is not restricted to nickel.⁵ Furthermore, many synthetic neutral MN₂S₂ small molecule models have been produced (where M = a variety of transition metals, most notably Ni, Fe, Co, Cu, Pt, and Zn) showing a considerable range in the binding capability of the N₂S₂ donor set.⁶ In particular, the nickel N₂S₂ complexes are known to be exceptional metalloligands, and there are several studies of their ability to nucleate bi, tri, and polymetallics through controlled thiolate sulfur aggregation.⁷ Nickel-containing small molecules have been prepared as mimics of the Ni_d site, Ni(CG C)²⁻, found in ACS.⁸ Riordan and co-workers have extensively studied the Ni(II) complex of the CGC⁴⁻ ligand, showing its ability to bind to a second low valent, "organometallic-like" nickel through the thiolate sulfur of Ni(CG C)²⁻.^{9,10}

Similar to biological studies, investigations using the neutral Ni(bme-daco) (bme-daco = bis(mercaptoethyl)diazacyclooctane) complex showed that the reactive thiolates had a greater specificity for copper over nickel and zinc, but there was no evidence of Ni^{II} ejection or Ni/Cu exchange from

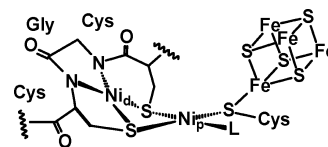


Figure 1. Acetyl CoA Synthase: Representation of the A-Cluster (Ni_{d,p} = distal and proximal relative to the 4Fe4S cluster).^{1,2}

the N₂S₂ core.^{3,11} These solution studies in combination with the biological studies discussed above piqued interest as to the reason why the M(Cysteine-X-Cysteine) biological motif is yet to be discovered with M = Cu^{II} and how the distal Ni(Cysteine-Glycine-Cysteine)²⁻ site of ACS is constructed *sans* Cu^{II}. In this regard, a baseline study of the stability and reactivity of biologically relevant CuN₂S₂²⁻-complexes via synthetic model complexes has been undertaken.

In nature, copper is found with diverse functions and binding sites reflecting its wide range of structural and redox utility in proteins.^{12,13} An additional aim of this study is to develop an understanding of how the unique electron transfer properties of biological copper in Cu/SR binding sites are achieved with no consequence for sulfur oxidation to disulfide. Frequently, the preparation of Cu^{II} monomeric complexes as synthetic analogues is challenged by a facile auto-oxidation process: 2Cu²⁺ + 2RS⁻ → 2Cu^I + RSSR.¹⁴ This is often followed by Cu^I binding to unreacted Cu^{II}-SR⁻ moieties producing complex aggregates.¹⁵ A number of N₃S pseudo-tetrahedral Cu^{II}-thiolate containing complexes have been produced utilizing scorpionate-type ligands as models of these systems.¹⁶ However, only a small number of structurally and spectroscopically characterized synthetic N₂S₂ square planar, copper(II)-thiolate complexes have been reported as monomers capable of withstanding copper reduction and aggregation (Figure 2).^{17,18} Although a number of these complexes model blue copper electron transfer sites, only the Krüger complex, Cu(phmi)²⁻ (phmi = N,N'-1,2-phenylenebis(2-mercapto-2-methylpropionamide)), contains amido donors that mimic the metal donor groups found in the M_d site of ACS.¹⁸ An advantage for the lack of aggregation of this model complex is that the ligand is composed of a bulky phenylene group on the N-to-N linker,

- (3) Bramlett, M. R.; Tan, X.; Lindahl, P. A. *J. Am. Chem. Soc.* **2003**, *125*, 9316–9317.
- (4) Seravalli, J.; Xiao, Y.; Gu, W.; Cramer, S. P.; Antholine, W. E.; Krymov, V.; Gerfen, G. J.; Ragsdale, S. W. *Biochemistry* **2004**, *43*, 3944–3955.
- (5) Nagashmia, S.; Nakasako, M.; Dohmae, N.; Tsujimura, M.; Takio, K.; Odaka, M.; Yoshida, M.; Kamiya, N.; Endo, I. *Nat. Struct. Biol.* **1998**, *5*, 347–351.
- (6) (a) Smees, J. J.; Miller, M. L.; Grapperhaus, C. A.; Reibenspies, J. H.; Darensbourg, M. *Inorg. Chem.* **2001**, *40*, 3601–3605. (b) Chiang, C.-Y.; Lee, J.; Dalrymple, C.; Sarahan, M. C.; Reibenspies, J. H.; Darensbourg, M. Y. *Inorg. Chem.* **2005**, *44*, 9007–9016. (c) Holland, P. L.; Tolman, W. B. *J. Am. Chem. Soc.* **2000**, *122*, 6331–6332. (d) Almaraz, E.; de Paula, Q. A.; Liu, Q.; Reibenspies, J. H.; Darensbourg, M. Y.; Farrell, N. P. *J. Am. Chem. Soc.* **2008**, *130*, 6272–6280.
- (7) (a) Wang, Q.; Marr, A. C.; Blake, A. J.; Wilson, C.; Schroeder, M. *Chem Commun.* **2003**, 22, 2776–2777. (b) Hatlevik, O.; Blanksma, M. C.; Mathrubootham, V.; Arif, A. M.; Hegg, E. L. *J. Biol. Inorg. Chem.* **2004**, *9*, 238–246. (c) Verhagen, J. A. W.; Tock, C.; Lutz, M.; Spek, A. L.; Bouwman, E. *Eur. J. Inorg. Chem.* **2006**, 23, 4800–4808. (d) Turner, M. A.; Driessen, W. L.; Reedijk, J. *Inorg. Chem.* **1990**, *29*, 3331–3335. (e) Golden, M. L.; Jeffery, S. P.; Miller, M. L.; Reibenspies, J. H.; Darensbourg, M. Y. *Eur. J. Inorg. Chem.* **2004**, 2, 231–236.
- (8) Rao, P. V.; Bhaduri, S.; Jiang, J.; Holm, R. H. *Inorg. Chem.* **2004**, *43*, 5833–5849.
- (9) Krishnan, R.; Riordan, C. G. *J. Am. Chem. Soc.* **2004**, *126*, 4484–4485.
- (10) (a) Green, K. N.; Jeffery, S. P.; Reibenspies, J. H.; Darensbourg, M. Y. *J. Am. Chem. Soc.* **2006**, *128*, 6493–6498. (b) Green, K. N.; James, W. D.; Cantillo, A. V.; Darensbourg, M. Y. *J. Organomet. Chem.* **2007**, *692*, 1392–1397.

- (11) Golden, M. L.; Rampersad, M. V.; Reibenspies, J. H.; Darensbourg, M. Y. *Chem. Commun.* **2003**, 15, 1824–1825.
- (12) Kraatz, H.-B.; Metzler-Nolte, N. In *Concepts and Models in Bioinorganic Chemistry*; Wiley: Weinheim, Germany, 2006; pp 364–395.
- (13) Solomon, E. I. *Inorg. Chem.* **2006**, *45*, 8012–8025.
- (14) (a) Miyoshi, K.; Sugiura, Y.; Ishizu, K.; Iitaka, H. *J. Am. Chem. Soc.* **1980**, *102*, 6130–6136. (b) Warner, L. G.; Ottersen, T.; Seff, K. *Inorg. Chem.* **1974**, *13*, 2819–2826. (c) Helton, M. E.; Chen, P.; Paul, P. P.; Tyeklar, Z.; Sommer, R. D.; Zakharov, L. N.; Rheingold, A. L.; Solomon, E. I.; Karlin, K. D. *J. Am. Chem. Soc.* **2003**, *125*, 1160–1161.
- (15) (a) Miller, M. L.; Ibrahim, S. A.; Golden, M. L.; Darensbourg, M. Y. *Inorg. Chem.* **2003**, *42*, 2999–3007. (b) Golden, M. L.; Whaley, C. M.; Rampersad, M. V.; Reibenspies, J. H.; Hancock, R. D.; Darensbourg, M. Y. *Inorg. Chem.* **2005**, *44*, 875–883.
- (16) John, E.; Bharadwaj, P. K.; Potenza, J. A.; Schugar, H. J. *Inorg. Chem.* **1986**, *25*, 3065–3069.
- (17) (a) Houser, R. P.; Tolman, W. B. *Inorg. Chem.* **1995**, *34*, 1632–1633. (b) Bharadwaj, P. K.; Potenza, J. A.; Schugar, H. J. *J. Am. Chem. Soc.* **1986**, *108*, 1351–1352. (c) Klein, E. L.; Khan, M. A.; Houser, R. P. *Inorg. Chem.* **2004**, *43*, 7272–7274.
- (18) Hanss, J.; Krüger, H. J. *Angew. Chem., Int. Ed. Engl.* **1996**, *23*, 2827–2830.

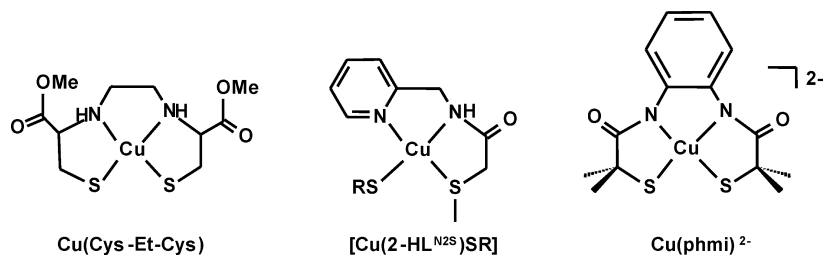
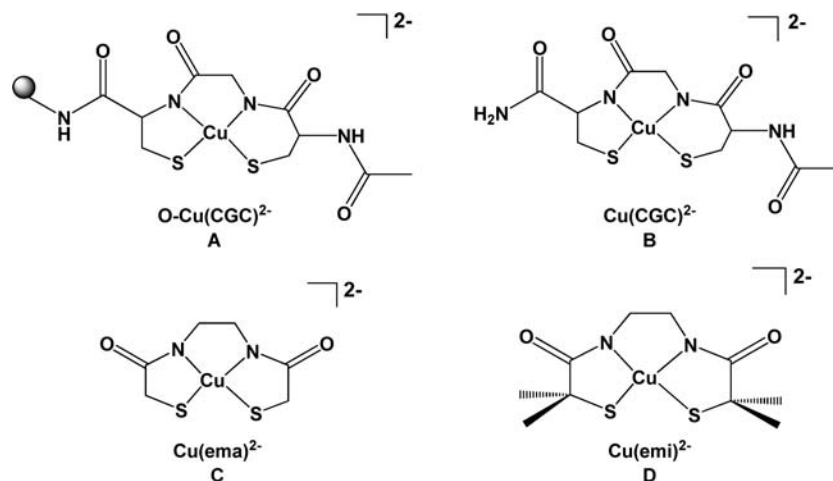


Figure 2. Examples of synthetic monomer $\text{Cu}^{\text{II}}\text{N}_2\text{S}_2$ and $\text{CuN}_2\text{SS}'$ complexes: $\text{Cu}(\text{Cys-Et-Cys}) = [\text{Dimethyl } N,N'\text{-ethylenebis(L-cysteinato)-S,S'}]\text{copper(II)}$, $[\text{Cu}(2\text{-HL}^{\text{N}_2\text{S}})\text{SR}] = 2\text{-methylthio-N-(2-pyridylmethyl)acetamide copper(II)}$; $\text{Cu}(\text{phmi})^{2-} = N,N'\text{-1,2-phenylenebis(2-mercapto-2-methylpropionamide)-copper(II)}$.^{17,18}

Chart 1



as well as gem-dimethyl groups on the aliphatic carbons adjacent to the thiolates.

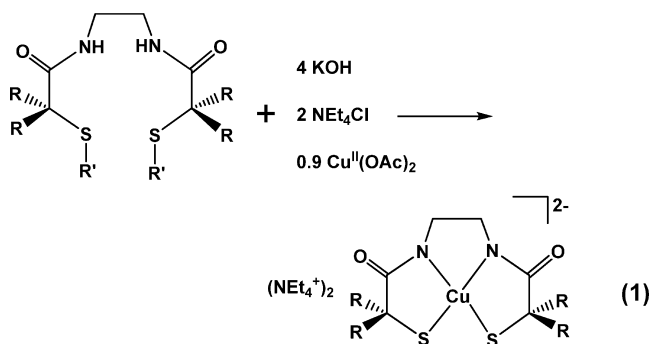
To investigate the prospect of a Cu^{II} in the $\text{Cys-Gly-Cys } \text{N}_2\text{S}_2^{4-}$ binding site of ACS and concomitantly avoiding aggregate formation as a consequence of redox processes, we have prepared the $\text{CuN}_2\text{S}_2^{2-}$ (**B**, **C**, and **D**) complexes shown in Chart 1, as well as a $\text{Cu}^{\text{II}}\text{-N}_2\text{S}_2^{2-}$ system (**O-Cu(CGCG)^{2-}**, **A**), tethered to a polymer scaffold reported to provide site–site isolation.¹⁰ The resin-bound system is used for investigating Ni/Cu exchange processes while preventing or impeding the formation of large aggregates.

Results and Discussion

Synthesis and Characterization of Resin-Free $\text{Cu}^{\text{II}}\text{N}_2\text{S}_2^{2-}$ Complexes: $\text{K}_2[\text{Cu}(\text{CGC})]$ (Complex **B), $[\text{Et}_4\text{N}]_2[\text{Cu}(\text{ema})]$ (Complex **C**), and $[\text{Et}_4\text{N}]_2[\text{Cu}(\text{emi})]$ (Complex **D**). Synthesis.** For solution studies, the *N*-acetylated and *C*-amidated Ac-CGC-NH_2 tripeptide was obtained by the Fmoc method of solid phase peptide synthesis followed by cleavage from the NovaSyn TGR (TGR = TentaGel Resin).¹⁰ The $\text{K}_2[\text{Cu}^{\text{II}}(\text{CGC})]$ complex, represented in Chart 1 as **B**, was prepared by addition of $\text{Cu}^{\text{II}}(\text{OAc})_2$ to a basic methanol solution of Ac-CGC-NH_2 in *N,N*-dimethylformamide (DMF) over a period of 15 min to minimize aggregate formation. The purple $\text{K}_2[\text{Cu}(\text{CGC})]$ complex, [ESI-MS ($[\text{Cu}(\text{CGC})]^- = 380.97 \text{ m/z}$ (100%), Calcd = 380.98 *m/z*), is air-sensitive but stable indefinitely when stored under N_2 as a solid. In contrast, decomposition occurs in methanol or DMF solutions after a few hours resulting in a highly insoluble yellow-brown solid. Its

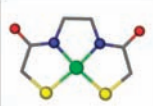
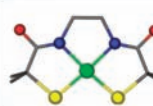

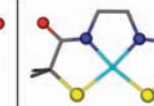
insolubility and mass spectral data suggest aggregate formation, likely resulting in *S*-oxidation and Cu^{II} reduction to Cu^{I} .^{14–16}

In previous studies of dianionic $\text{NiN}_2\text{S}_2^{2-}$ complexes, we have shown $\text{Ni}(\text{ema})^{2-}$ to model the $\text{Ni}(\text{CGC})^{2-}$ complex in terms of additional metal binding through *S*-based ligating ability.¹⁰ Because of the increased instability in solution and decomposition pathways of $\text{Cu}(\text{CGC})^{2-}$ versus the nickel analogue, synthetic analogues $[\text{Et}_4\text{N}]_2[\text{Cu}(\text{ema})]$ and $[\text{Et}_4\text{N}]_2[\text{Cu}(\text{emi})]$, (**C** and **D**, Chart 1), were prepared.



According to Eq 1, and similarly to the synthesis of the $\text{Cu}(\text{CGC})^{2-}$ complex, the air sensitive Et_4N^+ salts of **C** and **D** were prepared, recrystallized, and analyzed by electrospray ionization mass spectrometry (ESI-MS). Complexes **C** and **D** showed parent ion peaks at 266.93 and 323.00 *m/z*, respectively ($[\text{CuN}_2\text{S}_2]^- = 100\%$ shown in the Supporting Information, Figure S1). In the absence of air, the complexes

Table 1. Selected Distances (Å), Angles (deg), and Other Parameters of Interest for (Ni(ema)²⁻)²⁰, (Ni(emi)²⁻)⁸, Cu(ema)²⁻, and Cu(emi)²⁻ Anions

				
	[Et ₄ N] ₂ [Ni(ema)] ²⁰	[Et ₄ N] ₂ [Ni(emi)] ⁸	[Et ₄ N] ₂ [Cu(ema)]	[Et ₄ N] ₂ [Cu(emi)]
M-S _{avg} (Å)	2.170(1)	2.181(1)	2.2654(7)	2.233(4)
M-N _{avg} (Å)	1.857(3)	1.858(2)	1.946(2)	1.940(8)
S-M-S (°)	97.44(8)	99.10(3)	101.64(4)	102.32(15)
N-M-N (°)	85.6(2)	85.67(9)	83.45(14)	85.01(5)
S-M-N (°)	88.4(1)	87.66(7)	87.45(7)	86.2(3)
Deviation ^a (Å)	0.0000 (0.0086)	0.0064 (0.0072)	0.0000 (0.0033)	0.0000 (0.0000) ^c
T _d Twist ^b (°)	2.2	1.2	0.8	0.0

^a Mean deviation from the planes defined by the N₂S₂ (MN₂S₂) atoms. ^b T_d twist defined by the dihedral angle made by the intersection of planes N₂M and S₂M. ^c Observed planarity a product of the crystallographic symmetry.

are soluble and stable for at least 24 h in acetonitrile, methanol, DMF, and water solutions as demonstrated by invariant UV–vis spectra. The Evans' method of determining magnetic moments¹⁹ revealed a μ_{eff} of 1.52 μ_{B} for Cu(ema)²⁻ and 1.59 μ_{B} for Cu(emi)²⁻ indicating a Cu^{II} ion with one unpaired electron at room temperature in acetonitrile solution for each case. As the cyclic voltammograms, *vide infra*, show completely reversible Cu^{III/II} redox couples, and as the N₂S₂⁴⁻ type ligands have been shown by both Holm and Krüger to permit isolation of the M^{III} oxidation state in Ni and Cu complexes, we conclude that the deviation from the ideal magnetic moment of 1.73 μ_{B} is likely attributed to [Cu^{III}(ema)]⁻ or [Cu^{III}(emi)]⁻.^{18,20}

Structural Characterization of C and D. Dark purple crystals suitable for X-ray diffraction studies were obtained by layering concentrated acetonitrile solutions with diethyl ether. Despite attempts to maintain dry conditions, water molecules were found within the crystal forms. The molecular structures of **C** and **D** along with the nickel analogues [Et₄N]₂[Ni(ema)] and [Et₄N]₂[Ni(emi)], reported by Holm et al., are shown for comparison as ball and stick representations in Table 1.^{8,20} The MN₂S₂²⁻ (M = Ni, Cu) complexes contain a symmetry-imposed mirror plane perpendicular to the MN₂S₂ plane that bisects the N–C–C–N linker backbone. The Cu–S and Cu–N distances are similar to those reported for the Cu(phmi)²⁻ complex shown in Figure 2.¹⁸ Complex **D** has symmetry imposed, strict planarity while **C** has a mean deviation of ±0.0033 Å in the CuN₂S₂ plane. Despite the symmetry present in the molecule, inducing the planarity indicated above, elongated thermal parameters in the crystal structures of **C** and **D** may be suggestive of a slight tetrahedral twist in the ligand set. An interesting structural feature is the elongation of the M–S bond resulting in the expansion of the S–M–S angle in the Cu^{II} complexes compared to their Ni^{II} analogues. This increase in bond length is attributed to population of an antibonding orbital within the σ bonding orbital regime (*vide infra*). The

packing diagram of each structure (see Figure 3 and Supporting Information, Figure S5) shows that the MN₂S₂ complexes are linked via hydrogen bonds of interstitial water molecules; for example, molecules of **C** are linked through water molecules from the amido oxygen of one CuN₂S₂ unit to the thiolate sulfur of the next. These linkages create sheets composed of MN₂S₂ complexes and water molecules with the Et₄N⁺ cations separating each layer. Therefore, in the solid state no intermolecular CuN₂S₂²⁻ interactions are observed.

Reactivity. The copper complexes **B**, **C**, and **D** react with [Rh(CO)₂Cl]₂ similarly to NiN₂S₂^{x-} complexes ($x = 0, 2$).¹⁰ Examples of crystallographically characterized NiN₂S₂M-(CO)_x complexes are shown in Figure 4 as structures **E**, **F**, and **G**. Evidence for adduct formation with the CuN₂S₂^{x-} complexes as metalloligands is obtained from the two band $\nu(\text{CO})$ pattern observed in the FTIR spectra of solutions following mixing of the Cu and Rh reagents (Supporting Information, Figures S4 and S5). Table 2 compares the $\nu(\text{CO})$ values of the Rh(CO)₂⁺ adducts of the nickel complexes with the copper congeners. The Cotton–Kraihanzel force constants (k) are very similar; however, the interaction force constants (k_i) are slightly higher for Cu versus Ni,²¹ which could be related to the difference in the S–M–S bite angle noted in the crystallographic metric parameters (*vide supra*). Nevertheless the two $\nu(\text{CO})$ bands are of similar intensity in all cases, indicating carbonyls at about 90° angles. In the absence of crystals of the copper derivatives, IR measurements suggest that the copper–rhodium complex is analogous to the dimeric nickel derivative (**G**) shown in Figure 4,¹⁰ although the CuRh heterobimetallic, which would be analogous to **F** as shown below, cannot be ruled out.

Computational Details of Ni(ema)²⁻, Ni(emi)²⁻, Cu(ema)²⁻, and Cu(emi)²⁻. The gas-phase density-functional theory (DFT) computations of the Ni(N₂S₂)²⁻ complexes (B3LYP functional and 6-311G(d,p) basis set) and of the Cu(N₂S₂)²⁻ complexes (utilizing both unrestricted and

(19) (a) Evans, D. F. *J. Chem. Soc.* **1959**, 2003. (b) Grant, D. H. *J. Chem. Educ.* **1995**, 72, 39.

(20) Krüger, H.-J.; Peng, G.; Holm, R. H. *Inorg. Chem.* **1991**, 30, 734–742.

(21) Cotton, F. A.; Kraihanzel, C. S. *J. Am. Chem. Soc.* **1962**, 84, 4432–4438.

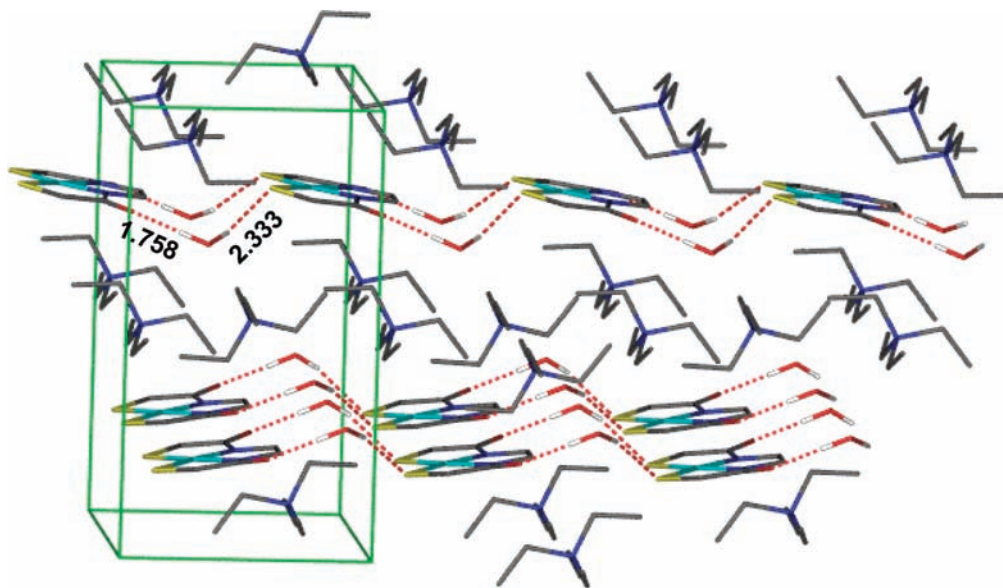


Figure 3. Crystal packing diagram of $[\text{Et}_4\text{N}]_2[\text{Cu}(\text{ema})] \cdot 2\text{H}_2\text{O}$ showing H-bonding and distances (Å) between $\text{CuN}_2\text{S}_2^{2-}$ molecules.

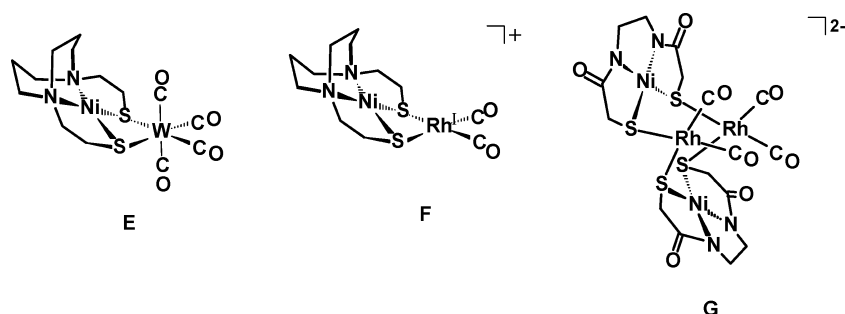


Figure 4. Examples of metal carbonyl derivatives derived from $\text{NiN}_2\text{S}_2^{x-}$ complexes ($x = 0, 2$): **E** = $\text{Ni}(\text{bme-daco})\text{W}(\text{CO})_4$, **F** = $\text{Ni}(\text{bme-daco})\text{Rh}(\text{CO})_2^+$, **G** = $[\text{Ni}(\text{ema})\text{Rh}(\text{CO})_2]_2^{2-}$.¹⁰

Table 2. Comparison of $\text{MN}_2\text{S}_2\text{Rh}(\text{CO})_2^{1-}$ Complexes ($M = \text{Cu}, \text{Ni}$) in DMF Solvent

$\text{MN}_2\text{S}_2^{2-}$	$\nu(\text{CO})$ (cm^{-1})	k ($\text{mdyn}/\text{\AA}$) ^a	k_i ($\text{mdyn}/\text{\AA}$) ^a
$\text{Cu}(\text{ema})^{2-}$	2061, 1982	16.51	0.64
$\text{Cu}(\text{emi})^{2-}$	2062, 1984	16.53	0.64
$\text{Cu}(\text{CGC})^{2-}$	2061, 1983	16.52	0.64
$\text{Ni}(\text{ema})^{2-}$	2056, 1990	16.53	0.54
$\text{Ni}(\text{emi})^{2-}$	2051, 1987	16.47	0.52
$\text{Ni}(\text{CGC})^{2-}$	2058, 1986	16.52	0.59

^a Cotton–Kraihanzel force constants, which utilizes a force field in which $k_c = k_c'/2 = k_i$ (k = stretching force constant, k_i = interaction force constant).²¹

restricted open shell B3LYP calculations and the 6-311G(d,p) basis set) resulted in optimized structures and metric parameters fully consistent with the crystallographic experimental results (see Supporting Information, Table S3).

The optimized structure of $\text{Ni}(\text{emi})^{2-}$ has nearly identical geometric parameters to the $\text{Ni}(\text{ema})^{2-}$ complex;^{22,23} therefore the following discussion is appropriate to both complexes. Figure 5 illustrates that the highest occupied molecular orbital (HOMO) and HOMO-1 molecular orbitals are close in energy, and are composed of metal-d and sulfur-p π -antibonding interactions, involving antisymmetric and

symmetric combinations of the sulfur p_z orbitals in the following linear combinations:

$$\text{HOMO-1: } M d_{yz} - (S p_z + S p_z)$$

$$\text{HOMO: } M d_{xz} - (S p_z - S p_z)$$

The slight energy difference could be explained in terms of the contribution from both the amido nitrogen and the oxygen atoms in the HOMO-1, whereas the oxygen atom interaction is absent in the HOMO.

Table 3 gives the atomic orbital contributions to the frontier molecular orbitals for the nickel and copper complexes. The values presented for sulfur and nitrogen refer to each of the two atoms. In both $\text{Ni}(\text{ema})^{2-}$ and $\text{Ni}(\text{emi})^{2-}$, the metal contribution to the HOMO is essentially the same; however, a slight difference is observed for the sulfur contributions. The HOMO-1 of both $\text{Ni}(\text{ema})^{2-}$ and $\text{Ni}(\text{emi})^{2-}$ complexes is composed of Ni d_{yz} character and p_z character from each sulfur and also a symmetric combination of the nitrogen p_z orbitals. The lowest unoccupied molecular orbital (LUMO) of $\text{Ni}(\text{emi})^{2-}$ consists of an antibonding σ -orbital set, in the xy plane. The HOMO–LUMO gap of $\text{Ni}(\text{emi})^{2-}$ is calculated to be 4.20 eV which is slightly higher than that of $\text{Ni}(\text{ema})^{2-}$, found to be 4.12 eV.^{22,23}

The frontier orbitals of $\text{Cu}(\text{ema})^{2-}$ and $\text{Cu}(\text{emi})^{2-}$ share the same fundamental characteristics with differences in

(22) Green, K. N.; Brothers, S. M.; Jenkins, R. M.; Carson, C. E.; Grapperhaus, C. A.; Darensbourg, M. Y. *Inorg. Chem.* **2007**, *46*, 7536–7544.

(23) Mullins, C. S.; Grapperhaus, C. A.; Kozłowski, P. M. *J. Biol. Inorg. Chem.* **2006**, *11*, 617–625.

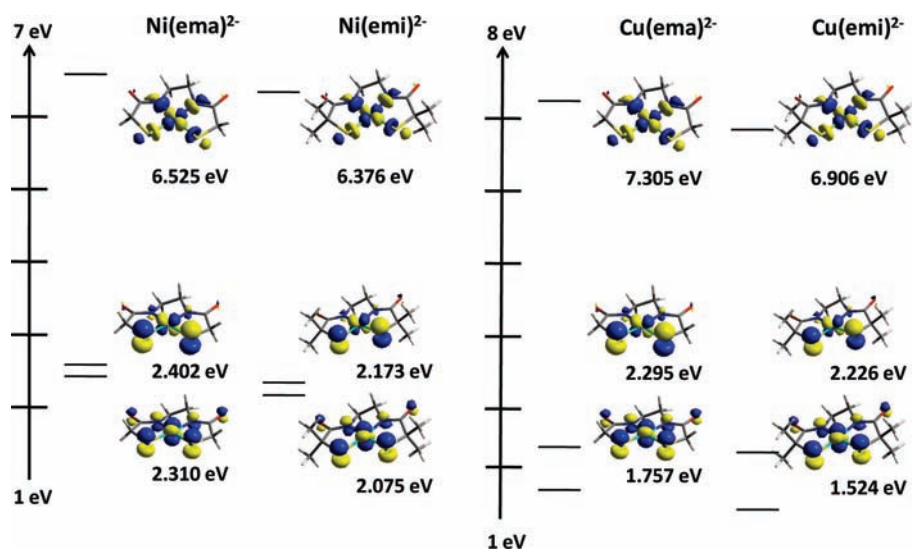


Figure 5. Frontier molecular orbitals of Ni(ema)²⁻,^{22,23} Ni(emi)²⁻, Cu(ema)²⁻, and Cu(emi)²⁻. For the nickel complexes, the orbitals descend in the order LUMO, HOMO, and HOMO-1. For the copper complexes, the orbitals descend in the order SOMO, HOMO, and HOMO-1.

Table 3. Atomic Orbital Contributions to Calculated Frontier Molecular Orbitals^a

	Ni(ema) ²⁻ ^{22,23}	Ni(emi) ²⁻	Cu(ema) ²⁻	Cu(emi) ²⁻
LUMO/SOMO	32% Ni	29% Ni	45% Cu	43% Cu
	14% S	11% S	12% S	12% S
	6% N	6% N	9% N	9% N
HOMO	40% Ni	39% Ni	4% Cu	4% Cu
	22% S	20% S	43% S	41% S
	2% N	1% N	0% N	0% N
HOMO-1	47% Ni	43% Ni	7% Cu	7% Cu
	14% S	14% S	35% S	34% S
	4% N	4% N	4% N	4% N

^a S and N contributions are given per atom.

orbital contributions from the copper and the ligand set. The orbital composition of the singly occupied molecular orbital (SOMO), similar to that of the LUMO of the corresponding Ni complexes, involves a σ -antibonding overlap of the d_{xy} orbital of copper with the p_{σ} orbitals of sulfur and nitrogen. The HOMO has a minor (4%) copper contribution to the antisymmetric M–S d_{π} - p_{π} overlap and a thiolate sulfur contribution of 41–43% each. These orbital compositions are different for the corresponding nickel complexes where a larger metal contribution is observed. For both Ni and Cu, the HOMO-1 is more delocalized relative to the HOMO. The HOMO-SOMO gaps of Cu(ema)²⁻ and Cu(emi)²⁻ are 5.01 and 4.68 eV, respectively, a trend analogous to the HOMO–LUMO gaps of the Ni(ema)²⁻ and Ni(emi)²⁻ complexes (*vide supra*).

The difference in metal orbital contributions to the HOMO and HOMO-1 between the nickel and copper complexes can be attributed to intrinsic metal properties, in that the bonding d orbitals of the copper(II) are stabilized in energy relative to nickel(II), while the antibonding d_{xy} , destabilized as a result of the ligand field symmetry, is indicated by the increase of copper character in the SOMO. Overall, the calculations indicate a greater degree of covalency in the metal–sulfur bond of the nickel complexes as compared to the copper most directly observed in the HOMO and HOMO-1 orbitals.

In general, computational structural parameters (described above) are corroborated by experiment. The most significant

differences between the Cu and Ni complexes appear in the M–S and M–N bond lengths, as well as the S–M–S and N–M–N angles. Because of the presence of a populated σ^* orbital, which is unpopulated in the Ni cases, bond lengths in the copper complexes are about 0.1 Å greater than those found in the analogous nickel complexes, and the S–M–S angle expands by approximately 5° for copper complexes. The distortions from planarity, as indicated by the $S_1N_1N_2S_2$ dihedral angle, are very small for the Ni complexes (3 to 4°), whereas for the Cu complexes a distortion in the form of a T_d twist is between 8.5 and 9.5°, indicating somewhat of a shift toward a pseudo-tetrahedral geometry which is likely for a d^9 metal ion. The fact that this is not observed in the experimental structures probably reflects crystallographically imposed symmetry. Nevertheless, the amidothiolate $N_2S_2^{4-}$ ligands are much more rigid binding sites as contrasted to the $N_2S_2^{2-}$ ligands.

Electrostatic Potential Maps and Mulliken Charges.

The electrostatic potential plots, as well as the Mulliken charges, for the $M(N_2S_2)^{2-}$ [$M = Ni^{II}, Cu^{II}; N_2S_2 = ema^{4-}, emi^{4-}$] series offer insight into the probable sites for charge-controlled, electrophilic and nucleophilic reactivity of the four complexes (see Figure 6 and Table 4). The overall charge delocalization imparted by the carboxamido unit on these dianionic NiN_2S_2 complexes as compared to the neutral NiN_2S_2 analogues was earlier noted. The negative charge of the carboxamido group is shared between both the nitrogen and the oxygen atoms, creating an iminolate contribution to the metal center.^{22,23} The Cu(ema)²⁻ and Cu(emi)²⁻ complexes display a greater degree of charge polarization as compared to the Ni^{II} congeners, implying that the Cu^{II} derivatives have less of a covalent interaction with the $N_2S_2^{4-}$ ligand set. This is seen by inspection of the electrostatic potential maps of Figure 6 where there are similar areas of positive and negative character on the sulfur, nitrogen, and oxygen atoms of the $N_2S_2O_2$ backbone for all four complexes. However, a major change in these four systems is seen by the amount of positive character on the copper in Cu(ema)²⁻

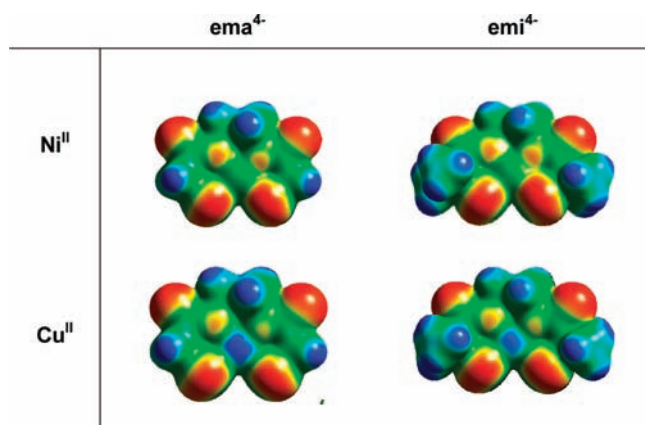


Figure 6. (From right to left) Electrostatic potential maps of $\text{Ni}(\text{ema})^{2-}$, $\text{Ni}(\text{emi})^{2-}$, $\text{Cu}(\text{ema})^{2-}$, and $\text{Cu}(\text{emi})^{2-}$ plotted at an isosurface value of 0.01. The range was taken from 1.00 (the most electropositive region, dark blue) to 0.33 (the most electronegative region, bright red). The view is oriented from the top onto the MN_2S_2 plane.

and $\text{Cu}(\text{emi})^{2-}$ versus the Ni^{II} analogues, indicating the greater ionicity in the former complexes. The Mulliken charges listed in Table 4 for the ema^{4-} and emi^{4-} metal complexes are entirely consistent with the electrostatic potential maps but they provide a more quantitative analysis of the charge distribution. For example, the polarization of charge in the copper systems is observed in the thiolate sulfur character which is in the range of -0.584 and -0.638 while the thiolate sulfurs of the nickel complexes are significantly more positive, -0.509 and -0.571 . This corresponds to a higher positive charge on copper of about 0.20 units as compared to nickel. There are no significant differences in the negative charge of the carboxyamido oxygen atoms throughout the series of complexes (between -0.511 and -0.520 , see Table 4). For complexes containing the same metal ion, the differences in the charges of the sulfurs and the metal are small and probably insignificant. Because of the asymmetry of the ligand set, the negative charges of the nitrogen and the oxygen atoms in the CGC^{4-} complexes are unequal (see Table 4).

Spectroscopic Characterization of $\text{K}_2[\text{Cu}(\text{CGC})]$, $[\text{Et}_4\text{N}][\text{Cu}(\text{ema})]$, and $[\text{Et}_4\text{N}]_2[\text{Cu}(\text{emi})]$. The copper coordination environments for **B**, **C**, and **D** were assessed by electronic absorption spectroscopy and electron paramagnetic resonance (EPR) spectroscopy. Table 5 shows the λ_{max} and extinction coefficients characteristic of the electronic absorption spectrum of each complex in the UV–visible region in acetonitrile solvent. The position and intensity of the high energy bands at ~ 320 and 290 nm in the $\text{Cu}(\text{ema})^{2-}$ and the $\text{Cu}(\text{emi})^{2-}$ complexes suggest charge transfer transitions whereas the moderate intensity ($\epsilon \sim 400\text{--}800$) of the low energy bands at ~ 400 nm and ~ 500 nm are likely $\text{S}_\sigma \rightarrow \text{Cu}$ and $\text{S}_\pi \rightarrow \text{Cu}$ transitions, respectively.^{12,13} Solomon and others noted that spectroscopic differences can be used to highlight structural dissimilarities between copper binding sites such as those in plastocyanin, nitrocyano, and synthetic metalloprotein active site models.^{12,17,18} For complexes **B**, **C**, and **D** the $\text{S}_\sigma \rightarrow \text{Cu}$ transitions are red-shifted relative to nitrocyano and are of a much lesser intensity.¹² The contour plots for the ground-state wave functions of $\text{Cu}(\text{ema})^{2-}$ and

$\text{Cu}(\text{emi})^{2-}$ illustrate that the $\text{S}-\text{Cu}$ bonding is dominated by a $\text{d}_\pi\text{-p}_\sigma$ sigma interaction which is considered to be weak owing to a poor $\text{d}_\pi\text{-p}_\sigma$ orbital energy match and is a likely explanation for the weak band intensity.

The $\text{S}_\sigma \rightarrow \text{Cu}$ transition of the Cu^{II} complexes around 400 nm is lower in energy than the corresponding transition in Ni^{II} complexes.²⁰ The relatively weak sigma interaction in the Cu^{II} complexes, when compared with Ni^{II} complexes, is indicated in the electrostatic potential diagram which shows a significant degree of charge separation and also in the longer $\text{M}-\text{S}$ bond lengths in the Cu^{II} complexes. Whereas the flat nature of the molecule would normally facilitate both sigma and pi overlap, in this case, the frontier molecular orbital diagram shows that there is a poor energy match between the p orbitals on sulfur and the d orbitals on copper.

The nature of the copper environment in **B**, **C**, and **D** was assessed by EPR spectroscopy. The X-band EPR spectra resulting from frozen DMF solutions (9 K) of the $\text{CuN}_2\text{S}_2^{2-}$ complexes show axial signals with $g_{\parallel} > g_{\perp} > 2.003$ which is the signature pattern expected for Cu^{II} ($S = 1/2$, $I = 3/2$) in a square planar environment with a $\text{d}_{x^2-y^2}$ or d_{xy} ground state (Supporting Information, Figures S2 and S3). The anisotropic spin-Hamiltonian parameters exhibit values in the region expected for N_2SX complexes where $\text{X} = \text{N}$, O , or S . When A_{\parallel} and g_{\parallel} values are compared with the 2N2S region in Peisach–Blumberg correlation diagrams²⁴ the observation is that values for **B**, **C**, and **D** complexes lie in the region between the 4S and 4N complexes but outside of the region delineated for 2N2S complexes of Cu^{II} .²⁴ This deviation is a consequence of larger g_{\parallel} values for **B**, **C** and **D** and is appreciable when compared to natural and artificial proteins although the degree of fit is improved when compared with the latter.²⁴ There are several factors that influence the values of A_{\parallel} and g_{\parallel} , and they may operate in concerted or opposing ways. Such factors include ligand charge, covalency, and geometry of the metal binding domain.

EPR spectra were recorded for **B**, **C**, and **D** in the coordinating solvent DMF; therefore, there is a strong likelihood that axial solvent coordination is influencing the g_{\parallel} values. It has been reported that axial coordination decreases the covalency in the axial bonds, resulting in the increased g_{\parallel} value observed for **B**, **C**, and **D**.²⁵ Assuming that the electric field around the Cu^{II} is unchanged going from liquid to frozen solution, then the increased g_{\parallel} value, which places the complexes outside of the delineated region for 2N2S complexes in the Peisach–Blumberg correlations,²⁴ could be rationalized by considering axial solvent coordination. This argument is supported by the calculated Mulliken charges (*vide supra*) which suggest that there is a high degree of charge polarization in the Cu complexes. The implication is that electron delocalization, reduced in the plane of the ligand atoms, is manifested as increased g_{\parallel} values. The magnitude of A_{\parallel} and g_{\parallel} depends not only on the nature of

(24) Peisach, J.; Blumberg, W. E. *Arch. Biochem. Biophys.* **1974**, *165*, 691–708.

(25) Hwang, J. S.; Hussain, M. S. *Transition Met. Chem.* **1987**, *12*, 214–218.

Table 4. Mulliken Charges on M/S/N/O Atoms in the Ni(ema)²⁻, Ni(emi)²⁻, Cu(ema)²⁻, and Cu(emi)²⁻ Anions

atom	Ni(ema) ²⁻	Ni(emi) ²⁻	Ni(CGC) ²⁻	Cu(ema) ²⁻	Cu(emi) ²⁻	Cu(CGC) ²⁻
M	+0.871	+0.858	+0.904	+1.068	+1.061	+0.982
S	-0.571/-0.571	-0.509/-0.509	-0.499/-0.495	-0.638/-0.638	-0.584/-0.584	-0.564/-0.563
N	-0.630/-0.630	-0.628/-0.628	-0.627/-0.644	-0.676/-0.676	-0.672/-0.672	-0.569/-0.680
O	-0.520/-0.520	-0.512/-0.512	-0.518/-0.425	-0.518/-0.518	-0.511/-0.511	-0.515/-0.424

Table 5. Summary of Electronic Absorption Spectra for Cu(ema)²⁻, Cu(emi)²⁻, Cu(CGC)²⁻ in CH₃CN Solvent

	UV-vis λ_{\max} (nm) (ϵ , M ⁻¹ , cm ⁻¹)			
Cu(CGC) ²⁻	294 (18 962)	322sh(13 450)	367 (933)	497 (422)
Cu(ema) ²⁻	293 (28 721)	320sh(22 115)	407 (1740)	510 (923)
Cu(emi) ²⁻	289 (25 254)	319sh(22 347)	407 (2125)	508 (886)

Table 6. Comparison of g_{\parallel} , g_{\perp} , and A_{\parallel} Values for CuN₂S₂²⁻ Complexes

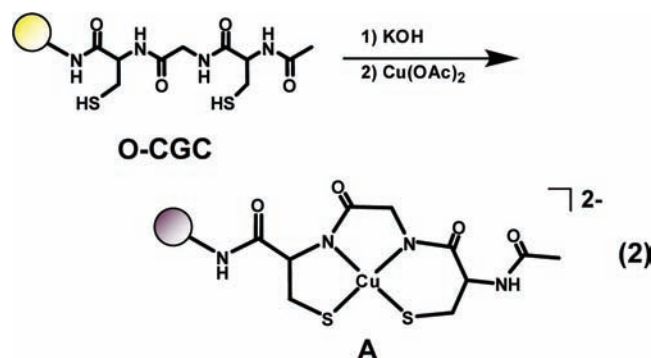
	g_{\parallel}	g_{\perp}	A_{\parallel} (cm ⁻¹)
Cu(CGC) ²⁻	2.185	2.105	186
Cu(ema) ²⁻	2.170	2.110	195
Cu(emi) ²⁻	2.220	2.120	175
O-Cu(CGC) ²⁻	2.230	2.100	195

the coordinating ligands but also on the type of adjacent atoms. Since the axial EPR spectrum displayed by **B**, **C**, and **D** is characteristic of Cu^{II} in a tetragonal environment and not representative of a sulfur-based radical, it is reasonable to suggest that the magnetic parameters indicate both N and S binding to copper. There is no significant variation in the EPR parameters for all three complexes (**B**, **C**, and **D**) indicating the structural similarities in copper binding geometries and ligand donor sets (Table 6).

Electrochemical Studies of C and D. Cyclic voltammograms of **C** and **D**, measured in DMF, display two redox events (a full scan of **C** is in Supporting Information, Figure S8). The response in the range of -800 to -1000 mV is assigned to the Cu^{III/II} redox couple, and its reversibility is verified by I_{pa}/I_{pc} values close to 1 (**C** = 0.957, **D** = 0.983) and by small ΔE values measured at 82 and 98 mV for **C** and **D**, respectively (Supporting Information, Table S2). An irreversible oxidation attributed to ligand decomposition is observed at more positive potentials as well (Supporting Information, Figure S8 and Table S2).

The cyclic voltammograms of the isolated reversible Cu^{III/II} redox couple of **C** and **D** are shown in Figure 7. To our knowledge, complex **D**, which is considered to have the most negative Cu^{III/II} couple reported to date at $E_{1/2} = -1.40$ V versus Fc^{+/0}, is 0.20 V more difficult to access compared to that of **C**. Although Cu^{III} is considered rare, access to the high valent cuprate state can be attributed to stabilization afforded by the highly negative and polarizable carboxamido nitrogens from the ligand set. This was first noted by Krüger and co-workers with the Cu(phmi)²⁻ complex ($E_{1/2} = -1.16$ V vs Fc^{+/0} in CH₃CN).¹⁸ Figure 7 shows that the potentials of the Cu^{III/II} couples of **C** and **D** are >350 mV more negative than the reversible Ni^{III/II} couples of the Ni(ema)²⁻ and Ni(emi)²⁻ complexes. This is consistent with the greater effective nuclear charge of Cu^{II} over Ni^{II} and further demonstrates, as discussed by Kitagawa, et al., how the choice of metal can be used to tune the properties of a biological ligand.²⁶

Synthesis, Characterization, and Reactivity of Resin-Bound O-Cu(CGC)²⁻, Complex A. The N-acetylated, resin-bound O-CGC⁴⁻ tripeptide was obtained by the Fmoc method of solid phase peptide synthesis as described above for complex **B** (*vide supra*).¹⁰ The potassium salt of the resin-bound copper complex O-Cu(CGC)²⁻ was prepared in a fritted syringe by the addition of 0.142 mmol/g of Cu^{II}(OAc)₂ (assuming a similar O-CGC⁴⁻ uptake capacity as was found in nickel studies)^{10b} to a DMF slurry of O-CGC⁴⁻ loaded beads producing a deep purple coloration within 10 min, (Eq 2). A schematic representation of the composition of the resin is given in Figure 8. The CGC⁴⁻ loaded beads/Cu^{II}(OAc)₂ slurry was agitated for an additional 50 min, then extensively washed with DMF, dichloromethane, and methanol solvents, and dried in vacuo. An EPR spectrum of the 1:1 copper/peptide reaction product was recorded (Figure 9a), and an axial spectrum, similar to **B**, **C**, and **D** was obtained. The measured values of the anisotropic spin-Hamiltonian parameters ($g_{\parallel} = 2.230$, $g_{\perp} = 2.100$, and $A_{\parallel} = 195$ G) correlate well with those of complexes **B**, **C**, and **D** (*vide supra*) suggesting an N₂S₂ coordination for Cu^{II}. The fact that the resin-bound complex possesses EPR characteristics similar to **B**, **C**, and **D** indicates that site isolation, rather than polynuclear products, has been achieved within the resin. A recent investigation involving resin-bound cysteine as part of the ligand system demonstrated the formation of a stable Ni^{II} complex as its Ph₂PCH₂CH₂PPh₂ derivative, O-(N-S)²⁻Ni(dppe).²⁹



When excess copper was added to the O-CGC/Cu^{II} loaded beads, an additional interaction was indicated by line broadening in the X-band EPR frozen solution spectrum (10 K, Figure 9b). An EPR spectrum of the resin and Cu²⁺ in the absence of peptide is also shown in Figure 9c. The higher g -values ($g_{\perp} = 2.110$ and $g_{\parallel} = 2.304$) correspond to an oxygen environment and are indicative of a PEG-Cu^{II} interaction.²⁴ A number of reports have shown that chelation

(26) This concept is discussed in greater detail in Kitagawa, T.; Dey, A.; Lugo-Mas, P.; Benedict, J. B.; Kaminsky, W.; Solomon, E. I.; Kovacs, J. A. *J. Am. Chem. Soc.* **2006**, *128*, 14448-14449.

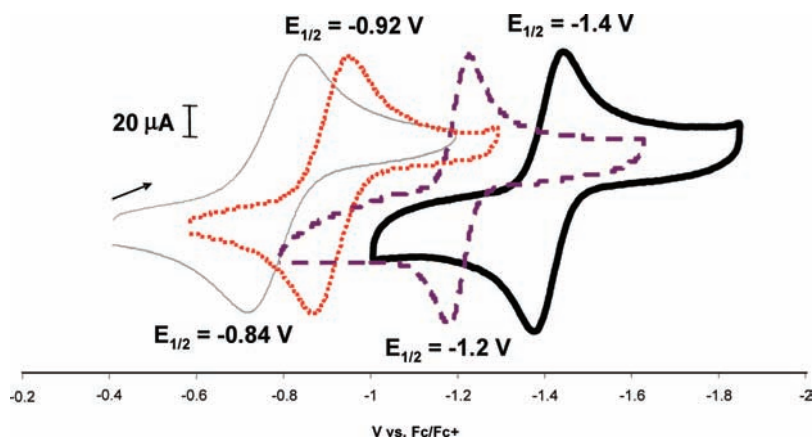


Figure 7. CV overlay of the Ni^{III/II} and Cu^{III/II} couples of [Et₄N]₂[Ni(ema)] (3.7 mM) (gray light line), [Et₄N]₂[Ni(emi)] (4.2 mM) (red dotted line), [Et₄N]₂[Cu(ema)] (4.0 mM) (purple dashed line), [Et₄N]₂[Cu(emi)] (2.3 mM) (black solid line) using DMF solvent at a scan rate of 100 mV/s, a Ag/AgNO₃ reference electrode, 0.1 M [t⁺Bu₄N][BF₄] electrolyte, and a glassy-carbon electrode.

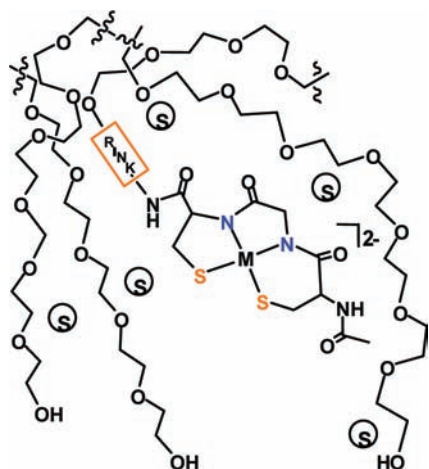


Figure 8. Schematic of the resin bound O-CGC/M²⁺ loaded beads. (S = solvent molecules, Rink linker = trialkoxybenzhydrylamine).

of various transition metal ions such as Rh^{III} by the PEG can occur.²⁷ Uptake of transition metals with an affinity for O-donors is not surprising in view of the fact that the TentaGel resin-beads are mainly composed of oxygen-rich PEG units.²⁸ Since 1 equiv of Cu(OAc)₂ results in O-Cu(CGC)²⁻, it is reasonable to conclude that binding of Cu^{II} by the CGC⁴⁻ moiety occurs preferentially and that excess Cu^{II} results in stable Cu-PEG interactions.

To further identify the presumed resin-bound O-Cu(CGC)²⁻, attempts were made to derivatize the CuN₂S₂ site with Rh(CO)₂⁺ since this procedure was effective in studies with NiN₂S₂²⁻.¹⁰ The $\nu(\text{CO})$ infrared spectrum (ATR-FTIR) obtained from the resulting purple-red beads on addition of a solution of [Rh(CO)₂Cl]₂ followed by DMF, methanol, and dichloromethane washes and drying in vacuo, showed two bands of equal intensity at 2066 and 1989 cm⁻¹. This indicates *cis*-CO moieties about 90° to one another (Supporting Information, Figure S4b) and donor capabilities that

are similar to the Cu(ema)²⁻ and Cu(emi)²⁻ complexes. An indication of the air-stability of the O-Cu(CGC)²⁻ beads was noted by their ability to react with Rh(CO)₂⁺ after 2 weeks of exposure to air. In contrast, the resin-free analogues, B, C, and D, decompose within minutes.

Metal Uptake Studies. Since the thiolates of Ni(CGC)²⁻ found in Acetyl CoA Synthase display a high affinity for both Cu^{II} and Ni^{II} and model studies of the synthetic, neutral NiN₂S₂ complexes gave similar results, exogenous metal binding and possible transmetalation reactions of Cu^{II} within the N₂S₂ core were investigated.

Nickel vs Copper Metalation. As a preliminary investigation to compare the affinity of Cu^{II} versus Ni^{II} for the O-CGC⁴⁻ site, a rudimentary competition study was performed. [The word “rudimentary” is used since for solubility reasons, two different sources of Cu and Ni are used and the nature of the metal ion species present in solution is not defined.]³⁰ Since aggregates may form in solution, the resin-bound analogue O-CGC⁴⁻ was used for this study. To a suspension of O-CGC⁴⁻ in DMF were added equimolar solutions of Cu(OAc)₂ and Ni(acac)₂ simultaneously. The contents of the flask containing the resin-bound peptide suspension were agitated for 1 h, collected via filtration, washed, and dried. An EPR spectrum of the orange-brown beads showed a signal corresponding to O-Cu(CGC)²⁻ but was difficult to quantify. On exposure of the beads to solutions of [Rh(CO)₂Cl]₂, the broad bands in the IR spectrum centered at 2065 and 1991 cm⁻¹ indicate a mixture of two or more species with the O-Cu(CGC)²⁻ adduct of Rh(CO)₂⁺ predominating.

The Cu/Ni competition experiment for O-CGC⁴⁻ experiment was repeated, and the suspension of beads and reagents was agitated for 6 h, collected via filtration, washed, and dried. The resulting concentration of nickel and copper within the beads was determined via Neutron Activation Analysis (Sample 1) and compared to samples of O-Ni(CGC)²⁻ (Sample 2) and O-Cu(CGC)²⁻ (Sample 3) produced from

(27) Ford, W. T.; Bergbreiter, D. E.; Waller, F. J.; Ekerdt, J. G.; Garrou, P. E.; Neckers, D. C.; Taylor, R. T.; Wulff, G.; Patchornick, A.; Nov, E.; Jacobson, K. A.; Shai, Y. In *Polymer Reagents and Catalysts*; ACS Symposium Series 308; American Chemical Society: Washington, DC, 1986; pp 13, 84–106.

(28) (a) Bayer, E. *Angew. Chem., Int. Ed. Engl.* **1991**, *30*, 113–129. (b) Sherrington, D. C. *Chem. Commun.* **1998**, 2275–2286.

(29) Desrochers, P. J.; Duong, D. S.; Marshall, A. S.; Lelievre, S. A.; Hong, B.; Brown, J. R.; Tarkka, R. M.; Manion, J. M.; Holman, G.; Merkert, J. W.; Vivic, D. A. *Inorg. Chem.* **2007**, *46*, 9221–9233.

(30) Autiessier, V.; Henderson, R. A. *Inorg. Chem.* **2008**, *47*, 6393–6403.

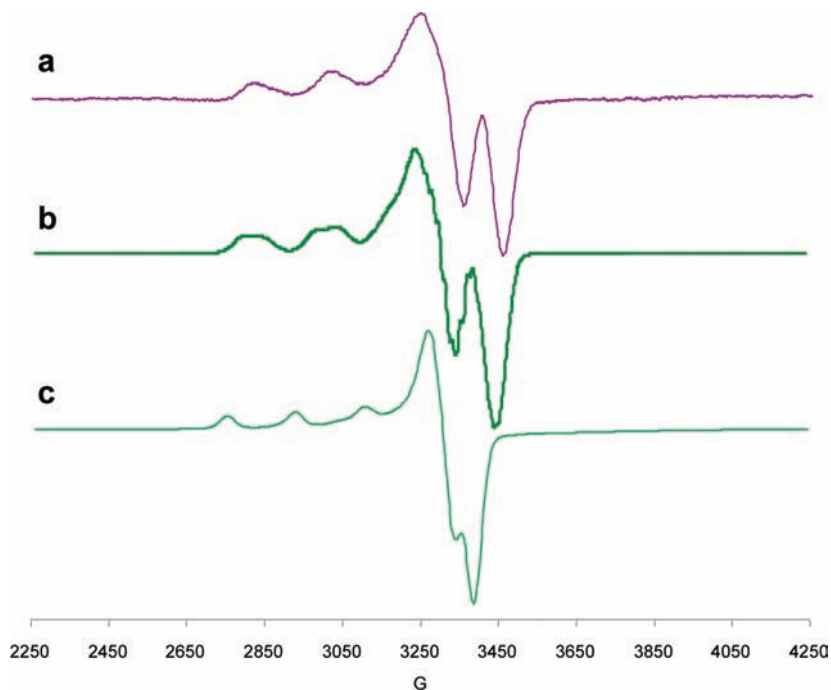


Figure 9. X-Band EPR spectra of (a) **O-Cu(CGC)²⁻**, complex A; (b) **O-CGC** incubated with 5 equiv of **Cu(OAc)₂**; (c) **O-NH₂** incubated with **Cu(OAc)₂** (spectra are obtained from dried beads packed into an EPR tube at 9 K and 9.75 GHz.) (**O** = NovaSyn TGR Beads).

Table 7. Concentration (mmol/g) of **Cu^{II}** or **Ni^{II}** Immobilized by **O-CGC⁴⁻** Determined by Neutron Activation Analysis Studies

sample	[nickel]	[copper]	[total]
1 O-CGC + Ni/Cu	0.069	0.114 (0.09 8) ^a	0.183
2 O-Ni(CGC)²⁻	0.142		0.142
3 O-Cu(CGC)²⁻		0.158 (0.142) ^a	0.158

^a Value obtained assuming 0.016 mmol/g attached to PEG.

the same batch of **O-CGC⁴⁻**. As shown in Table 7, when presented with both copper(II) and nickel(II) as the salts described above, both metals are bound, and the overall uptake of copper is greater than that of nickel resulting in a Cu/Ni ratio of 1.7:1. (This overall Cu/Ni uptake ratio however does not consider the issue of two sites within the resin beads that bind copper, *vide infra*.) The EPR spectrum of the orange-brown beads from Sample 1 showed a signal corresponding to **O-Cu(CGC)²⁻**.

As discussed earlier, in addition to the **O-CGC⁴⁻** copper-binding sites the PEG moiety can interact with copper, which could account for the slightly higher metal concentration in Sample 3 relative to Sample 2. Earlier studies with good reproducibility demonstrated a 1:1 correlation of **O-CGC⁴⁻** and **Ni²⁺** uptake;^{10b} hence we can assume that the copper-only sample has about 0.02 mmol/g **Cu^{II}** taken up in the PEG. If this assumption is correct, then the mixed-metal sample contains about 0.10 mmol/g **Cu^{II}** and a Cu/Ni ratio of 1.4:1. We cannot account for the discrepancy of the total metal uptake in Sample 1 and the amount of Cu taken up in Sample 3, and we do not know if this discrepancy indicates the error in the experiment. To this end, further analytical studies are underway. Nevertheless it is clear that both Cu and Ni compete for the **O-CGC⁴⁻** site.

The addition of 20 equiv of **Ni(acac)₂** to purple beads of **O-Cu(CGC)²⁻** resulted in no color change over the course of 6 h. Following washes and vacuum drying the resulting

EPR spectrum displays the axial signal previously assigned to **O-Cu(CGC)²⁻** further indicating that there is no significant exchange of **Ni²⁺** for **Cu²⁺**. The reverse experiments (i.e., exchange of **Cu²⁺** for **Ni²⁺**) attempting opposite exchange were also unsuccessful. Furthermore, under the conditions described above the thiolates of the **O-Ni(CGC)²⁻** and **O-Cu(CGC)²⁻** do not produce stable paramagnetic, multimetallic species when exposed to exogenous **Cu^{II}** or **Ni^{II}** in the form of **CuCl₂**, **Cu(OAc)₂**, **NiCl₂**, **Ni(acac)₂**, or **Ni(OAc)₂**.

Conclusions

The synthesis of new and stable dianionic **[Cu^{II}N₂S₂]²⁻** complexes has been described along with characterization including ESI-MS, UV-vis, EPR, and X-ray diffraction studies. The UV-vis and EPR data show that the complexes have a **Cu^{II}** center with two amido nitrogen and two thiolate sulfur donors provided by the ligands **emi⁴⁻**, **ema⁴⁻**, and **CGC⁴⁻**. The conclusions drawn from solution spectroscopy are corroborated by two solid state structures which show the **Cu^{II}** is in a square planar **N₂S₂** arrangement. The metal carbonyl derivatives show that the thiolate reactivity with **Rh(CO)₂⁺** of these **CuN₂S₂²⁻** complexes parallels the well-studied **NiN₂S₂** analogues. The **CuRh** bimetallic series also reveals that **Cu(ema)²⁻**, **Cu(emi)²⁻**, and **Cu(CGC)²⁻** are equal in donor ability. These results are reflected in the electrostatic potential maps derived from DFT calculations. As the EPs and Mulliken charges indicate a greater M-S charge separation when M = Cu, the ionicity within **M(N₂S₂)²⁻** is greater than when M = Ni. Nevertheless, the greater negative charge on sulfur does not correspond to a greater donor ability as indicated by the **M(N₂S₂)Rh(CO)₂⁻** complexes.

Synthesis of **O-Cu(CGC)²⁻** using previously reported methodology for the **O-Ni(CGC)²⁻** species produces dark purple beads that are stabilized against decomposition with

O₂.¹⁰ The immobilized O-Cu(CGC)²⁻ complex can be spectroscopically identified through EPR signals. Electron paramagnetic spectroscopy also showed that Cu^{II} binds to the underivatized TentaGel beads in the absence of the CGC⁴⁻ unit, presumably to the ether oxygen donors of PEG. Nevertheless, the capture of Cu^{II} by the CGC N₂S₂⁴⁻ units surpasses the Cu-PEG interaction. Derivatization with the Rh(CO)₂⁺ unit qualitatively shows that the same reactivity as observed in solution may occur resin-bound, further confirming that the Cu(CGC)²⁻ is immobilized.

Metal uptake studies showed that Cu^{II} and Ni^{II} are stable once in the N₂S₂ core, that is, transmetalation or metal ion exchange with Ni(acac)₂ and Cu(OAc)₂ as source of Cu^{II} and Ni^{II}, respectively, does not occur. Furthermore, multi-metallic species formed by thiolates bridging to Ni^{II} or Cu^{II} were not observed using the acac or acetato sources for exogenous Ni or Cu. Thus, the reactivity with Rh(CO)₂⁺ indicates the requirement for stabilizing ligands on the exogenous metal ion for producing bimetallic species such as O-Cu(CGC)Rh(CO)₂¹⁻.

Despite obvious caveats to the competitive metal uptake studies described above, we conclude that the N₂S₂⁴⁻ ligating unit, either free in solution or immobilized in a matrix, has a slight preference for Cu^{II} over Ni^{II}. A reasonable conclusion with regard to the ACS active site is that the biosynthetic pathway responsible for constructing the distal site of ACS must be selective for nickel insertion or copper exclusion, or both. We note that no biological Cu^{II} sites composed of the Cys-X-Cys ligand set have been reported to date. However, examples of Ni, Fe, and Co are known for enzymes with strikingly similar N₂S₂ ligands albeit with quite different biological roles. As our studies indicate a strong similarity between Ni^{II} and Cu^{II} in a N₂S₂⁴⁻ donor environment, and, in fact, a slight preference for Cu^{II} binding, an eventual sighting of a Cys-X-Cys-Cu^{II} moiety will not be surprising.

Experimental Procedures

Methods and Materials. General Procedures. Solvents were purified according to standard procedures and were freshly distilled under N₂ prior to use or purified and degassed via a Bruker solvent system.³¹ Other reagents were purchased from commercial sources and used as received unless noted.

Standard Fmoc Merrifield techniques were employed for all peptide syntheses. Fmoc-Cys(Mmt)-OH and Fmoc-Gly-OH were obtained from NovaBioChem. The solid supports, NovaSyn TGR resin-beads (Novabiochem) averaging 90 μm in diameter, are composed of polystyrene with cross-linking via divinylbenzene and grafted with polyethyleneglycol bearing a Rink linker (Rink = trialkoxybenzhydrylamine) as the free amine termini (0.4 mmol/g loading). Plastic-fritted syringes, 10 mL, were used as reaction vessels to facilitate the multiple additions and removal of reagents and wash solvents. Mixing of beads and reagents was accomplished by an automated shaker. Synthesis of resin-bound Cys-Gly-Cys (O-CGC⁴⁻) was performed as described previously.¹⁰

Syntheses of air sensitive Ni^{II} complexes were performed under anaerobic conditions using distilled/degassed solvents and standard Schlenk line techniques under an argon atmosphere. The [Et₄N]₂-

[Ni(ema)] and [Et₄N]₂[Ni(emi)] complexes were prepared following published procedures and used in cyclic voltammetry (CV) analysis to be consistent with conditions used for the new complexes reported herein.²⁰

Physical Methods. Solution infrared spectra were recorded on a Bruker Tensor 27 FTIR spectrometer using 0.1 mm NaCl sealed cells. The Pike MIRacle attachment from Pike Technologies was used for Attenuated Total Reflectance Infrared Spectra for solid state samples. UV-vis spectra were recorded on a Hewlett-Packard HP8452A diode array spectrometer. Mass spectrometry (ESI-MS) was performed by the Laboratory for Biological Mass Spectrometry at Texas A&M University. Elemental analyses were performed by the Canadian Microanalytical Services, Ltd., Delta, British Columbia, Canada. Cyclic voltammograms were obtained under an Ar atmosphere at 22 °C using a BAS100W potentiostat equipped with a 3.0 mm glassy carbon working electrode, a platinum wire auxiliary electrode, and Ag/AgNO₃ reference electrode. Measurements were performed in a DMF solution with 0.1 M [Bu₄N][BF₄] as supporting electrolyte. Ferrocene was used as an internal standard and reported relative to NHE (Fc/Fc⁺ = +692 mV vs NHE).³² EPR spectra were obtained with a Bruker ESP 300 spectrometer equipped with an Oxford ER910 cryostat operating at 10 K. Samples were 1 mM in analyte in DMF and frozen in liquid N₂ prior to recording the EPR spectra at 10 K. The g values reported were as simulated using the WinEPR Simfonia program.³³ Magnetic moments were determined utilizing the Evans method using a mixed solvent system of CD₃CN and CH₃CN.¹⁹ Measurements were taken by ¹H NMR using an Inova 300 MHz NMR spectrometer.

Structure Solution and Refinement. For **C** and **D**, a BRUKER D8 GADDS general-purpose three-circle X-ray diffractometer was employed for sample screening and data collection. The goniometer was controlled using the GADDS software suite (Microsoft Win 2000 operating system). A 0.7 mm nylon loop was dipped in the sample. The mounted tube was then placed on the diffractometer and in a cold nitrogen stream (Oxford) maintained at 280 K. The sample was optically centered with the aid of a video camera such that no translations were observed as the sample was rotated through all positions. The detector was set at 12 cm from the sample (MWPC Hi-Star Detector, 1024 × 1024 pixel). The X-ray radiation employed was generated from a Cu sealed X-ray tube (K_α = 1.54184 Å with a potential of 40 kV and a current of 40 mA) and filtered with a graphite monochromator in the parallel mode (175 mm collimator with 0.5 mm pinholes).

The beam intersection coordinates were compared to the corundum (Al₂O₃) standard coordinates, and changes were made accordingly. Single data frames were taken at widths of -179° in θ (continuous rotation on φ: Gandolfi Scan) with an exposure time of 5 s. Three frame sets at 20, 55, and 90° 2-θ settings were collected. The data was reduced by area integration methods to produce a single powder diffraction pattern for each frame. Merging the individual powder diffraction patterns in the program EVA produced a single one-dimensional pattern, which is reported. The parameters are listed in Supporting Information, Table S1.

For **C** and **D**, the integrated intensity information for each reflection was obtained by reduction of the data frames with the program SAINT V6.63.³⁴ The integration method employed a three-dimensional profiling algorithm, and all data were corrected for

(32) Connelly, N. G.; Geiger, W. E. *Chem. Rev.* **1996**, *96*, 877–910.

(33) WINEPR SIMFONIA, version 1.25; Bruker Analytische Messtechnik GmbH: Rheinstetten, Germany, 1996.

(34) (a) SAINT V6.63, Program for Reduction of Area Detector Data; Bruker Axs Inc.: Madison, WI. (b) Sheldrick, G. M. SADABS, Program for Absorption Correction of Area Detector Frames; Bruker Axs Inc.: Madison, WI.

(31) Gordon, A. J.; Ford, R. A. *The Chemist's Companion*; Wiley and Sons: New York, 1972; pp 429–436.

Lorentz and polarization factors, as well as for crystal decay effects. Finally the data was merged and scaled to produce a suitable data set. The absorption correction program SADABS was employed to correct the data for absorption effects. X-Seed was employed for the final data presentation and structure plots.³⁵ The tetraethylammonium cation and water molecules in each structure were found to be disordered between two positions. The anions were modeled by employing local bond distance restraints and included in the final refinement. CCDC reference numbers: 691889 and 691890.

Computations. DFT calculations were performed using a hybrid functional (the three-parameter exchange functional of Becke (B3)³⁶ and the correlation functional of Lee, Yang, and Parr (LYP)³⁷) (B3LYP) as implemented in Gaussian 03.³⁸ For each calculation, all atoms were optimized via the use of the 6-311g(d,p) basis set. Because of the paramagnetic nature of the model copper complexes, an unrestricted open-shell calculation was initially performed; however, to prevent spin contamination inherent in the unrestricted open-shell calculations, restricted open-shell calculations were also investigated. Optimized bond lengths and angles in these two methods were in all cases nearly identical. Cartesian coordinates for the starting input geometry of Ni(ema)²⁻ were extracted from the crystallographic structure, and the models of Ni(emi)²⁻ and the copper analogues were modified by adding the gem-dimethyl groups or changing the metal center, respectively. A frequency calculation was performed alongside each geometry optimization to ensure the stability of the ground state as ascertained by the absence of imaginary frequencies. Graphical visualizations of the electron density of the individual molecular orbitals and the electrostatic potentials were first generated as cube files from Gaussian, and these images were implemented into and viewed by the Cerius2 software package.³⁹ Optimized geometries of each of the complexes were imported into and visualized with JIMP2 and can be located in the Supporting Information.⁴⁰ Geometric parameters were extracted from the optimized structures by use of the GaussView program.⁴¹ For each complex in this text, the energies have been converted from values in hartrees to electron volts.

Synthesis of O-Cu(CGC)²⁻, Complex A. Deprotection of the TentaGel-bound, N-acylated, Mmt Cys-S-protected Ac-CysGlyCys-NH₂ tripeptide was accomplished via a 1:94:5 mixture of trifluoroacetic acid/dichloromethane/triisopropyl silane as described for

the synthesis of O-Ni(CGC)²⁻.¹⁰ Following washes (3 × 5 mL each) with pure dichloromethane and methanol solvent, a basic solution of Cu(OAc)₂ in 5 mL of 50:50 methanol/dichloromethane was introduced to the resin bed. The light-yellow TentaGel beads changed to a deep purple after 10 min. After 50 min, the Cu^{II} supernatant solution was expelled, and the beads were again washed with methanol, dichloromethane, and diethyl ether solvent until the residual washes were completely colorless. The purple beads were dried in vacuo and stored in a vacuum desiccator.

Synthesis of O-Cu(CGC)Rh(CO)₂¹⁻. In an analogous manner to the preparation of O-Ni(CGC)Rh(CO)₂¹⁻, a sample of O-Cu(CGC)²⁻, purple in color, was placed in a fritted syringe and swelled in DMF. A yellow dichloromethane solution of [Rh(CO)₂Cl]₂ was added resulting in dark red beads after 30 min. The beads were washed thoroughly with dichloromethane, methanol, and diethyl ether (3 × each) and then dried in vacuo. ATR-FTIR on solid, dried beads: ν(CO) = 2061s, 1983s cm⁻¹.

Synthesis of [K]₂[Cu(CGC)], Complex B. The H₂CGC (20 mg, 0.062 mmol) ligand and KOH (13.92 mg, 0.0248 mmol) were combined in 20 mL of DMF and allowed to stir for 20 min. To this was added dropwise a blue solution of Cu(OAc)₂ (15.6 mg, 0.0610 mmol in MeOH). The reaction mixture developed into a mauve purple after 15 min and was allowed to stir overnight. A light purple solid was obtained after precipitation with Et₂O. Yield 16.3 mg (70.0% yield). Absorption spectrum (CH₃CN): λ_{max} (ε, M⁻¹ cm⁻¹) 232 (26,185), 294 (18,962), 322sh (13,450), and 367(930) nm. ⁻ESI-MS: m/z 380.9314 [M]⁻.

Synthesis of [Et₄N]₂[Cu(ema)], Complex C. In a degassed Schlenk flask N,N'-ethylenebis(2-mercaptoacetamide) (2.09 g, 4.61 mmol), KOH (1.5 g, 27.8 mmol), and tetraethyl ammonium chloride (1.65 g, 10.0 mmol) were combined with 100 mL of methanol and magnetically stirred for 30 min. To this a bright blue methanol (100 mL) solution of Cu(OAc)₂ (0.8 g, 4.3 mmol) was added dropwise over the course of 5 min. The mixture was stirred for 15 min during which time the light yellow solution changed to maroon and then purple. After 1.5 h additional reaction time, the solvent was removed in vacuo, and the residue was redissolved in about 40 mL of CH₃CN. The solution was filtered through a Celite pad and reduced to 20 mL. A second filtration using filter paper wrapped around a cannula and secured with copper wire produced a deep purple solution. A solid was obtained from the filtrate by addition of 250 mL of diethyl ether. (1.74 g, 83% yield) Absorption spectrum (CH₃CN): λ_{max} (ε, M⁻¹ cm⁻¹) 233 (24,880), 293 (28,700), 320sh (22,100), 407 (1740) nm. ⁻ESI-MS: m/z 266.9275 [M]⁻. Anal. Calcd (found) for C₂₂H₄₈N₄CuO₂S₂: C 50.01 (49.75), N 10.60 (10.57), H 9.16 (9.30).

Synthesis of [Et₄N]₂[Cu(emi)], Complex D. The solids N,N'-ethylenebis(2-benzylthio)isobutyramide (1.61 g, 4.62 mmol), KOH (1.5 g, 27.8 mmol), and tetraethyl ammonium chloride (1.65 g, 10.0 mmol) were dissolved in 200 mL of CH₃OH and stirred for 30 min under a blanket of Ar. The slow addition of a MeOH solution of Cu(OAc)₂ (0.8 g, 4.3 mmol) to this solution followed by stirring at room temperature for 30 min produced a red solution. The solution was allowed to stir for an additional 30 min and filtered through a Celite pad; the solvent was removed in vacuo, and the residue taken up in about 40 mL of CH₃CN. The solution was filtered through Celite pad and reduced to 20 mL. A second filtration using a paper filter wrapped around a cannula and secured with copper wire produced a deep purple solution. (1.36 g, 74% yield). Crystals suitable for X-ray diffraction were obtained at -10° by layering a concentrated CH₃CN solution with hexane and then ether. Absorption spectrum (CH₃CN): λ_{max} (ε, M⁻¹ cm⁻¹) 231 (23,799), 294 (25,250), 319sh (21,300), and 413 (2120) nm. ESI-MS: m/z

- (35) Barbour, L. J. *J. Supramol. Chem* **2001**, *1*, 189–191; X-Seed - A Software tool for supramolecular crystallography.
 (36) Becke, A. D. *J. Chem. Phys.* **1993**, *98*, 5648.
 (37) Lee, C.; Yang, W.; Parr, R. G. *Phys. Rev.* **1988**, *37*, 785.
 (38) Frisch, M. J.; Trucks, G. W.; Schlegel, H. B.; Scuseria, G. E.; Robb, M. A.; Cheeseman, J. R.; Montgomery, J. A., Jr.; Vreven, T.; Kudin, K. N.; Burant, J. C.; Millam, J. M.; Iyengar, S. S.; Tomasi, J.; Barone, V.; Mennucci, B.; Cossi, M.; Scalmani, G.; Rega, N.; Petersson, G. A.; Nakatsuji, H.; Hada, M.; Ehara, M.; Toyota, K.; Fukuda, R.; Hasegawa, J.; Ishida, M.; Nakajima, T.; Honda, Y.; Kitao, O.; Nakai, H.; Klene, M.; Li, X.; Knox, J. E.; Hratchian, H. P.; Cross, J. B.; Bakken, V.; Adamo, C.; Jaramillo, J.; Gomperts, R.; Stratmann, R. E.; Yazyev, O.; Austin, A. J.; Cammi, R.; Pomelli, C.; Ochterski, J. W.; Ayala, P. Y.; Morokuma, K.; Voth, G. A.; Salvador, P.; Dannenberg, J. J.; Zakrzewski, V. G.; Dapprich, S.; Daniels, A. D.; Strain, M. C.; Farkas, O.; Malick, D. K.; Rabuck, A. D.; Raghavachari, K.; Foresman, J. B.; Ortiz, J. V.; Cui, Q.; Baboul, A. G.; Clifford, S.; Cioslowski, J.; Stefanov, B. B.; Liu, G.; Liashenko, A.; Piskorz, P.; Komaromi, I.; Martin, R. L.; Fox, D. J.; Keith, T.; Al-Laham, M. A.; Peng, C. Y.; Nanayakkara, A.; Challacombe, M.; Gill, P. M. W.; Johnson, B.; Chen, W.; Wong, M. W.; Gonzalez, C.; and Pople, J. A. *Gaussian 03*, Revision C.02; Gaussian, Inc: Wallingford CT, 2004.
 (39) *Cerius2*, version 3.0; MSI: Cambridge, U.K.
 (40) (a) Hall, M. B.; Fenske, R. F. *Inorg. Chem.* **1972**, *11*, 768–779. (b) Manson, J.; Webster, C. E.; Pérez, L. M.; Hall, M. B. <http://www.chem.tamu.edu/jimp2/index.html>.
 (41) Dennington, R., II; Keith, T.; Millam, J. *GaussView*, Version 4.1; Semichem, Inc.: Shawnee Mission, KS, 2007.

323.0042 [M]⁻. Anal. Calcd (found) for C₂₆H₅₆N₄CuO₂S₂·H₂O: C 50.33 (50.24), N 9.75 (9.72), H 9.03 (9.02).

Synthesis of [Et₄N]_x[Cu(ema)Rh(CO)₂]_x. Under an argon blanket, the purple solid, [Et₄N]₂[Cu(ema)] (20 mg, 0.037 mmol), was suspended in 20 mL of DMF. After 30 min stirring the solid was completely dissolved to give a yellow-red solution. A yellow solution of [Rh(CO)₂Cl]₂ (7.373 mg, 0.0189 mmol) was then added dropwise. After stirring for 2 h the resulting red-brown solution showed $\nu(\text{CO}) = 2061, 1982 \text{ cm}^{-1}$. A brown solid was obtained following precipitation with diethyl ether. Absorption spectrum (DMF): $\lambda_{\text{max}} (\epsilon, \text{M}^{-1} \text{ cm}^{-1})$ 270(27,610) and 330(18,610) nm.

Synthesis of [Et₄N]_x[Cu(emi)Rh(CO)₂]_x. To a red solution of [Et₄N]₂[Cu(emi)] (20 mg, 0.034 mmol) in 20 mL of DMF, a yellow solution of [Rh(CO)₂Cl]₂ (7.4 mg, 0.019 mmol) was added dropwise. The resulting brown-red solution provided $\nu(\text{CO}) = 2062, 1984 \text{ cm}^{-1}$. A brown solid was obtained following precipitation with diethyl ether. Absorption spectrum (DMF): $\lambda_{\text{max}} (\epsilon, \text{M}^{-1} \text{ cm}^{-1})$ 289(25,260) and 390(18,540) nm.

Acknowledgment. We acknowledge financial support from the National Science Foundation (CHE-0616695 to

M.Y.D, MCB 0542291 to D.A.R.) with contributions from the R.A Welch Foundation (A-0924 to M.Y.D.) and the National Institutes of Health (Chemistry-Biology Interface Training Grant to K.G. T32GM008523). We sincerely thank the TAMU X-ray crystallography facility (Drs. Nattamai Bhuvanesh and Joseph H. Reibenspies), The Laboratory for Molecular Simulation at Texas A&M University (Dr. Lisa Perez), and the Laboratory for Biological Mass Spectrometry (Dr. Shane Tichy) for their expert assistance in this work.

Supporting Information Available: Crystallographic data for **C** and **D** in both CIF and table format and a packing diagram for **D**, electrochemical data as both cyclic voltammograms and in table format, additional EPR and IR spectra of Cu^{II} complexes, and computational data including metric parameters and optimized structures. This material is available free of charge via the Internet at <http://pubs.acs.org>.

IC801628R